Electrospun Fibrous Scaffolds with Multiscale and Photopatterned Porosity

Harini G. Sundararaghavan, Robert B. Metter, Jason A. Burdick*

The structural and mechanical properties of tissue engineered environments are crucial for successful cellular growth and tissue repair. Electrospinning is gaining wide attention for the fabrication of tissue engineered scaffolds, but the small pore sizes of these scaffolds limit cell infiltration and construct vascularization. To address this problem, we have combined electrospinning with photopatterning to create multiscale porous scaffolds. This process retains the fibrous nature of the scaffolds and permits enhanced cellular infiltration and vascularization when compared to unpatterned scaffolds. This is the first time that photopatterning has been utilized with electrospun scaffolds and is only now possible with the electrospinning of reactive macromers.

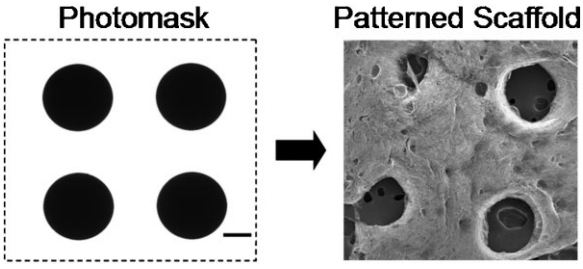

Introduction

Scaffolds are being developed for tissue engineering with precise structural and mechanical properties, as these features are now identified as being important in tissue development and maturation. Often, the use of synthetic materials is hindered by the complexity of native tissues and the need to tailor materials to the tissue of interest with respect to cell adhesion, mechanics, and porosity. In order to improve the successful integration and application of synthetic materials through manipulation of scaffold features, processing techniques such as microfluidics,[1,2] photolithography,[3,4] electrospinning,[5–7] laser ablation,[8] gas foaming,[9] and particulate leaching[10,11] have been used. The pore size and overall porosity of scaffolds are particularly important for cell infiltration and diffusion of nutrients and waste, and the design of optimal structures has been a major hurdle for tissue engineering therapies.[12–14] One processing technique, electrospinning, is gaining much attention because it produces scaffolds with a fibrous, porous structure that mimics the size scale of the native extracellular matrix (ECM); however, the small pore sizes of these scaffolds may limit cell infiltration and construct vascularization.[6,15,16]

Electrospinning has been widely used to create nanoscale fibers from a range of natural and synthetic materials.[6,17–22] This process involves ejecting a polymer solution from a charged needle until the electrical force overcomes the surface tension of the polymer to obtain polymer fibers that are collected on either a grounded plate or a rotating mandrel for alignment.[19] The fiber diameter and porosity of the scaffold can be controlled by changing parameters such as polymer flow rate, voltage, distance between the needle and the plate, and polymer concentration in the solution.[19] However, cell infiltration is limited in these structures due to dense fiber packing, particularly in aligned fibers, and techniques such as inclusion of sacrificial fibers,[6] combining micro- and nanoscale fibers,[23] including poragens,[15] or directly electrospinning in the presence of cells[24] have been investigated to overcome this problem. Some success has been observed, but limitations still exist because these techniques may alter the scaffold integrity and mechanics and the resulting porosity is still

H. G. Sundararaghavan, R. B. Metter, J. A. Burdick
University of Pennsylvania, Department of Bioengineering, 210 S 33rd Street, Philadelphia, PA 19104, USA
Fax: +1 215 573 2071; E-mail: burdick2@seas.upenn.edu

DOI: 10.1002/mabi.200900363

insufficient for construct vascularization. Additionally, patterning methods previously used with polymer materials such as microcontact printing[25] and dip pen lithography[26] have been adapted to electrospinning systems, but are mainly used to alter the scaffold surface and not the scaffold porosity. One promising technology for pore formation is photopatterning,[27] where a reactive macromer solution containing a photoinitiator is exposed to light through a mask and polymerization only occurs where light is transmitted. Enhanced resolution may also be obtained with directed light exposure via multi-photon lasers. This method was previously used to pattern channels ranging from 200 to 500 μm (actual pore dimensions were 360–730 μm) in poly(2-hydroxyethyl methacrylate) (poly-HEMA) gels with a combined sphere templating process.[27] However, these scaffolds do not exhibit ECM-like fibers, which is one of the main advantages of electrospinning. Only recently has electrospinning been performed with reactive macromers that have the potential to undergo a photopatterning process.[7] Thus, our novel approach combines photopatterning with electrospinning hyaluronic acid (HA), where we are able to produce polymer scaffolds with ECM-like fibrous structures, as well as macro-channels that support enhanced cellular infiltration and vascularization.

This technique is compatible with many reactive macromers that can be electrospun and also undergo a photoinitiated radical polymerization (e.g., methacrylated HA, MeHA). HA is a naturally occurring, linear polysaccharide made of alternating D-glucuronic acid and *N*-acetyl-D-glucosamine that is enzymatically degradable, important in many cellular functions including attachment, proliferation, and migration and is readily modified through its hydroxyl groups with methacrylation.[5,28,29] When crosslinked, HA networks have tunable mechanical properties (via changes in amount of methacrylation or macromer concentration)[30] and degradation can be controlled by adding a hydrolytically degradable moiety.[31] In our process, MeHA can be electrospun with a photoinitiator (Irgacure 2959) and carrier polymer [poly(ethylene oxide), PEO] to obtain fibrous scaffolds (non-aligned or aligned when spun on a rotating mandrel) that can subsequently be photocrosslinked and swollen to form fibrous hydrogels. If a photomask is used during the photocrosslinking step, crosslinking is controlled spatially and unreacted macromer (areas blocked from light) can be washed from the network to obtain macro-channels.

Experimental Part

Macromer Synthesis

MeHA was synthesized by reacting methacrylic anhydride (20-fold excess, Sigma) with a 1 wt.-% sodium hyaluronate (molecular weight = 74 kDa, Lifecore, Chaska, MN) in deionized (DI) H_2O solution adjusted to pH = 8 with 5 N NaOH on ice for 24 h, as previously described.[30] After reaction, the polymer was purified by dialysis against water for 48 h and then lyophilized to produce the final product. The percent methacrylation (percentage of HA repeat units with a methacrylate group) can be adjusted based on the amount of methacrylic anhydride added to the reaction and was determined to be ≈30% with ^{1}H NMR (Bruker Advance 360 MHz, Bruker, Billerica, MA) for this study. To promote cell adhesion, MeHA was modified with adhesive peptides through the addition reaction of thiol-terminated RGD peptide (GCGYGRGDSPG, Genscript, Piscataway, NJ) with the methacrylate groups for a final concentration of 10^{-3} M RGD in the samples. RGD peptide and MeHA were reacted overnight in triethanolamine buffer, dialyzed against DI H_2O for 48 h, and lyophilized to obtain MeHA-RGD.

Electrospinning HA Scaffolds

MeHA was co-spun with PEO (MW 900 kDa, Sigma) at 2 and 3 wt.-%, respectively. The polymer solution (HA, PEO, and 0.05 wt.-% I2959 in water) was ejected at 1.2 mL · h^{-1} using a syringe pump (KD Scientific) through a 12 cm long 18-gauge needle charged to 22 kV onto a grounded flat plate or a rotating mandrel (2 inch diameter, ≈10 m · s^{-1}) at a distance of 15 cm. To quantify fiber size and view morphology, scaffolds were imaged using scanning electron microscopy (SEM, JEOL 7500F HRSEM, Penn Regional Nanotechnology Facility) and fiber size was measured using NIH Image J (v1.42) with 100 measurements taken per SEM image for each condition.

Scaffold Crosslinking

Polymerization was accomplished by exposing as-spun MeHA mats in a purged nitrogen chamber to ≈10 mW · cm^{-2} 365 nm light (Omnicure S1000 UV Spot Cure System, Exfo Life Sciences Division, Mississauga, Ontario, Canada) with a collimating adapter for 5 min either directly or through a photomask with circular patterns. Subsequently, scaffolds were immersed in DI H_2O to remove unreacted MeHA and PEO (carrier polymer) to obtain either uniform or patterned fibrous HA scaffolds. Scaffolds were washed for 24 h (3 solution changes) to encourage removal of PEO and to reach equilibrium swelling. For SEM analysis, scaffolds were snap frozen in liquid nitrogen and lyophilized.

Mechanical Analysis

Rectangular samples (5 × 30 mm^2, ≈500 μm thick when dry) were cut from electrospun mats, both aligned and non-aligned scaffolds, in the parallel and transverse fiber direction (for aligned scaffolds), and crosslinked prior to testing. The scaffold thickness was determined using a custom built near frictionless linear variable differential transformer (LVDT) probe and platform apparatus capable of measuring sample thickness down to 0.01 mm. The specimen gauge length and width were determined using digital calipers. Samples were tested to failure at a constant strain rate of 0.1% using an Instron 5848 Microtester equipped with a 50 N load

Macromolecular Journals
DOI: 10.1002/mabi.200900363

cell (Instron, Canton, MA). The tensile modulus was calculated from the linear region of the stress/strain curve and the initial geometry of the sample. For testing of patterned scaffolds, patterned and control scaffolds were crosslinked, rinsed in DI H_2O to remove non-crosslinked polymer and PEO, and lyophilized prior to testing.

Cellular Interactions

For in vitro adhesion and spreading cell studies, HA scaffolds were electrospun as above onto methacrylated glass coverslips ($22 \times 22\ mm^2$) for 1 h (≈60 μm thick), crosslinked, washed with DI H_2O for 24 h, and sterilized under a germicidal lamp for 30 min. Human mesenchymal stem cells (MSCs, Lonza Corporation, Walkersville, MD) were expanded in growth media (α-MEM, 10% FBS, 1% L-glutamine and penicillin streptomycin) and seeded on scaffolds at a density of 100 000 cells/well in a 6-well tissue culture plate. Cells were allowed to attach for 24 h, fixed in 10% formalin for 30 min, washed three times for 5 min in wash buffer (1% BSA, 0.5% Triton-X), incubated in fluorescein isothiocyanate (FITC)-phalloidin ($0.66\ \mu g \cdot mL^{-1}$, Invitrogen, Carlsbad, CA) to visualize actin filaments, incubated in diamidino-2-phenylindole (DAPI, $0.4\ \mu L \cdot mL^{-1}$, Invitrogen) to visualize cell nuclei, and imaged using a Zeiss HBO 100 (Thornwood, New York) inverted fluorescent microscope.

For in vivo assessment, hydrated constructs ($n = 2$ per group and rat) were implanted subcutaneously in male Sprague-Dawley rats after pattern formation and hydration. Rats were anesthetized with isoflurane, and six subcutaneous pockets were made using an incision and blunt dissection. One electrospun scaffold was placed in each of these pockets and the wound was closed with sterile stainless steel skin clips. After 1 week, scaffolds and surrounding tissue were harvested and processed using standard histological techniques, stained with hematoxylin and eosin, and imaged using a Zeiss Axioskop 40 (Thornwood, New York) upright light microscope equipped with an AxioCam HRc camera. Animals were cared for according to a protocol approved by the University of Pennsylvania Institute for Animal Care and Use Committee.

Results and Discussion

HA has been previously electrospun with a range of carrier polymers, including PEO, gelatin, and zein, to increase solution viscosity.[22,32,33] We spun HA with PEO, due to its compatibility with our washing steps, and were able to obtain fibrous scaffolds with smooth fibers by spinning a solution of 2% MeHA (≈30% methacrylation), 3% PEO, and 0.05% I2959 in water and subsequent crosslinking with $\approx 10\ mW \cdot cm^{-2}$ ultraviolet light for 5 min. SEM images of scaffolds, both aligned and non-aligned are shown in Figure 1(A). The fibers were smooth and uniform in appearance and the average fiber diameters of non-aligned and aligned scaffolds were 230 ± 77 and 218 ± 47 nm, respectively. Upon hydration, the fibers swelled in water as PEO dissolved into the solution, yet the fiber morphology remains as observed in SEM images of a non-aligned scaffold that was lyophilized after hydration [Figure 1(A)]. When tested in tension (dry), the non-aligned HA scaffold exhibited a modulus of 56.5 ± 9.6 MPa compared to 79.8 ± 5.5 MPa (parallel to fiber direction) and 4.43 ± 0.76 MPa (transverse to fiber direction) for aligned scaffolds [Figure 1(A)]. These differential values for the aligned scaffolds tested in both directions indicate a high degree of

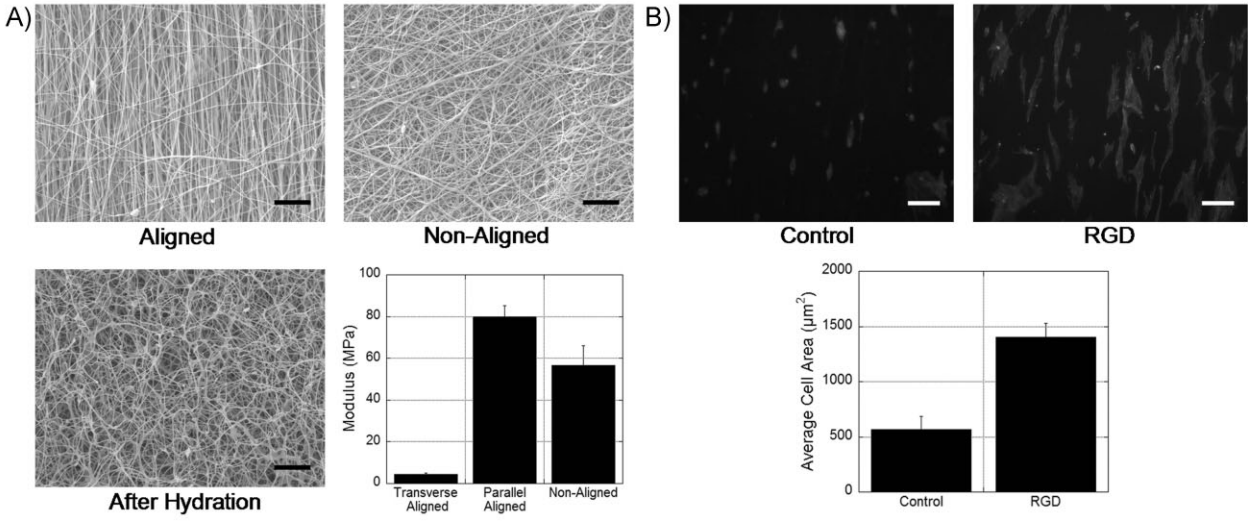

Figure 1. (A) SEM images of electrospun HA scaffolds aligned, non-aligned, and non-aligned after hydration (removal of unreacted HA and PEO) and lyophilization (scale bars = 10 μm). Tensile moduli of as-spun scaffolds that are either non-aligned or aligned (tested in both transverse and parallel directions). The moduli were all statistically significant ($p < 0.05$, ANOVA) between groups. (B) MSC adhesion on either unmodified (control) or RGD-modified electrospun HA scaffolds, illustrating the importance of biological cues on cellular interactions (scale bars = 100 μm). DAPI staining to visualize nuclei and FITC-phalloidin staining to visualize actin filaments shown. The average cell area increased significantly ($p < 0.05$, ANOVA) when HA was modified with RGD.

anisotropy. As expected, hydration and removal of PEO significantly decreased the mechanics of the scaffolds; non-aligned scaffold mechanics decreased to 311.0 ± 31.0 kPa.

HA hydrogels are inherently non-adherent to cells, particularly in the presence of PEO. In order to enhance cell interactions and spreading on HA scaffolds, HA was modified with a ubiquitous cell adhesion peptide, RGD, prior to electrospinning. This method has been previously shown to be an effective way in increase cell attachment and spreading on HA scaffolds.[34] As a representative anchorage dependent cell, MSCs were seeded on electrospun HA scaffolds after hydration. Cell adhesion and spreading were visually greater on scaffolds containing the adhesive peptide, with greater organization of actin filaments, as indicated by fluorescence [Figure 1(B)]. When quantified, a nearly 3-fold increase in spreading was observed for cells seeded onto the peptide containing gels. These results indicate that normally non-adhesive fibrous gels can be modified to enhance cellular interactions for both in vitro and in vivo applications.

To facilitate the formation of patterns in the scaffolds, a photomask (arrays of circular pores of either 250 or 500 μm diameter) was placed between the scaffold and the light during crosslinking [see schematic representation in Figure 2(A)]. After crosslinking, scaffolds were submerged in deionized water for 24 h at 37 °C and rinsed three times for removal of PEO and unreacted HA macromer. The ability to electrospin and wash scaffolds in the same solution, in this case deionized water, is imperative for the ability to photopattern electrospun scaffolds. Macro-channels were successfully formed in electrospun scaffolds with pore sizes of 165 ± 26 and 333 ± 38 μm for the 250 and 500 μm size mask features, respectively [Figure 2(B)]. Actual pore dimensions may be smaller than photomask dimensions due to light scattering, which can occur when light passes through the glass slides and fibers during crosslinking, and with swelling of the fibrous scaffolds after patterning and washing. To limit light scattering, crosslinking was performed with a collimated light and in a nitrogen environment to prevent quenching of free radicals by oxygen. In this study, the photopatterning method was demonstrated on non-aligned scaffolds; however, these techniques are translatable to aligned scaffolds as well. The ability to control mechanical anisotropy may be important for future tissue engineering applications of these materials, depending on the tissue. SEM images of the scaffolds show that the pores go through the entire scaffold thickness, match the general dimensions and shape of the mask features, and that a fibrous structure remains at the pore walls even after washing (Figure 3). The maintenance of scaffold architecture is essential to preserve the

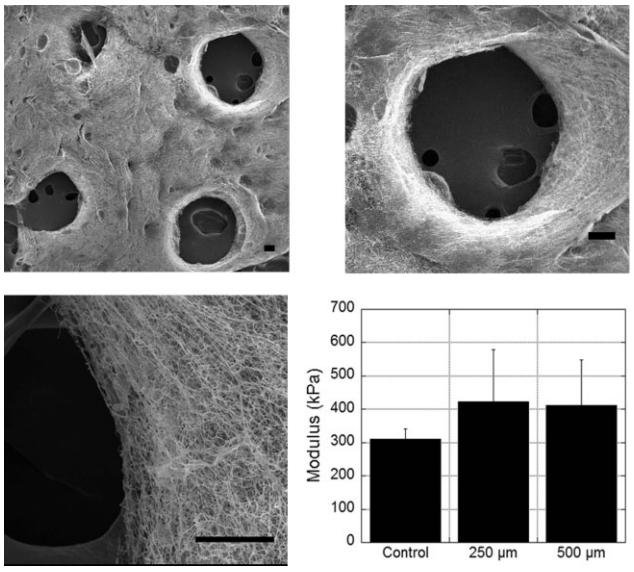

Figure 3. SEM images of scaffold structure at various magnifications after removal of unreacted HA and PEO, illustrating pore formation and stability of fibers during processing [scale bars = 100 μm (top 2 images) or 50 μm (bottom left)]. Bottom right: Modulus of patterned scaffolds (250 or 500 μm pores) after processing and drying compared to uniform scaffolds. There were no statistical differences ($p > 0.05$, ANOVA) between any of the scaffolds.

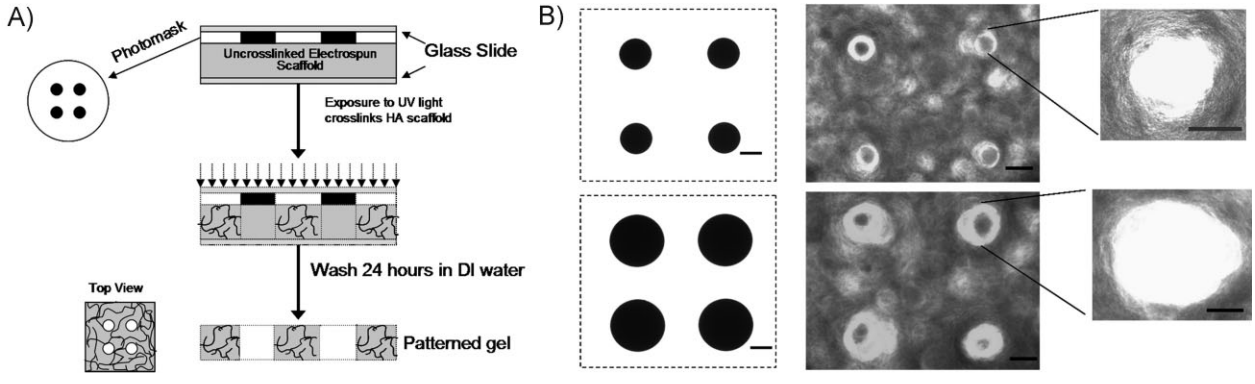

Figure 2. (A) Schematic representation of technique to photopattern macro-channels into electrospun scaffolds using light transmittance through masks. (B) Light micrographs of photomasks and top-view of patterned HA scaffolds (scale bars = 100 μm).

Macromolecular Journals
DOI: 10.1002/mabi.200900363

utility of the fibrous structure in cellular adhesion and organization. When the uniform and patterned non-aligned scaffolds were tested in tension, there were no statistical differences in the moduli of the dried non-aligned scaffolds that were crosslinked uniformly or those that contained channels (Figure 3). Importantly, this indicates that the bulk mechanics of the scaffolds are not compromised when this processing technique is used; however, these samples only had an array of four channels in them and the results may be different depending on the number and spacing of the channels. Additionally, it is important to note that cell-level mechanics should not be affected by photopatterning and processing methods.

To assess the utility of the scaffold channels to enhance cellular infiltration, both uniform and patterned scaffolds were implanted after hydration subcutaneously in vivo in rats. After 1 week, the scaffolds and surrounding tissue were harvested, sectioned using standard histological procedures, and stained with hematoxylin and eosin to view cell infiltration (Figure 4). It should be noted that the HA also stains with this process, but differences in nuclei staining are evident in the scaffolds. This model is useful to obtain general information on cellular infiltration into scaffolds and how it is altered by changing the scaffold macro-porosity. It is evident from the histology that there was very little cell infiltration (~100 μm) into the uniform fibrous scaffolds. As others have noted, it is likely that the dense packing of the fibers may be inhibitory to cell infiltration through the micro-porosity at this time point. Potentially, this could be enhanced with time and scaffold degradation.

In both patterned scaffolds (different channel dimensions), a significant increase in cell infiltration is observed and there are no regions where acellular scaffold remains (Figure 4). Typically, cellular infiltration only occurs to a depth of several hundred μm in these fibrous scaffolds, which is dependent on a number of material processing parameters, and is insufficient for the filling of thick constructs. However, our hypothesis was that macro-channels would decrease the length scales for cell infiltration into the scaffold (i.e., migration from the channel walls in addition to at the surface) and the bulk cellular uniformity would be enhanced. Our findings indicate that this is likely the case since all parameters were constant beyond the presence of scaffold channels. It should also be noted that large vascular structures are present throughout the scaffolds when the channels were included, but not in uniform scaffolds. At this point we have not performed a detailed study on the influence of specific channel size or frequency on cellularization, although rapid cell occupation occurred with all scaffolds investigated, and we have not targeted these materials for a specific application.

The cytocompatibility and versatility of HA make it an ideal candidate for tissue engineering applications, yet this

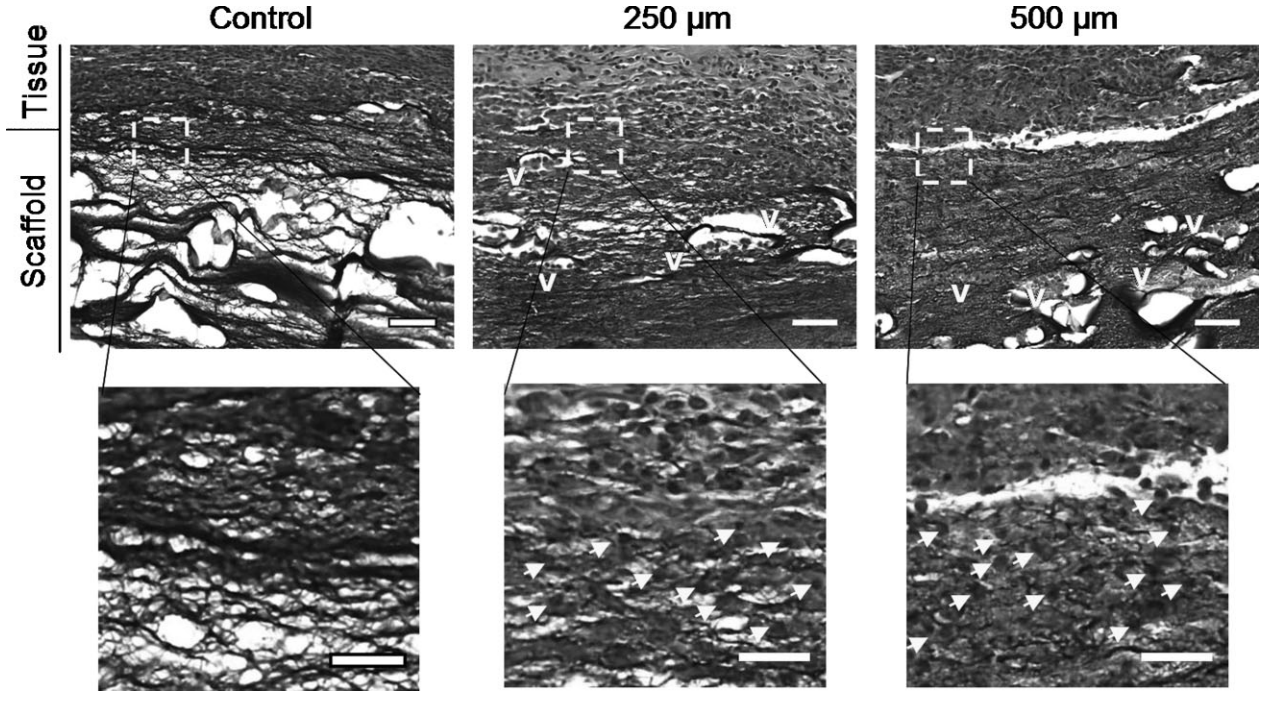

Figure 4. Representative images of cellular infiltration into electrospun scaffold implants 1-week post-implantation at either low (top, scale bar = 200 μm) or high (bottom, scale bar = 100 μm, regions from boxed area in less magnified images) magnification (V = vascular structures, arrows indicate representative nuclei). Although the control scaffolds stain with the dye, they are acellular and do not contain vascular structures, whereas both patterned macro-porous scaffolds show increased cell infiltration into the scaffold.

technology is applicable to a wide range of photocrosslinkable materials.[35] Only recently has photopolymerization been combined with electrospinning and thus, this is the first time that photopatterning of macro-channels has been performed with fibrous structures. Using this system, we are able to control micro- and macro-porosity with spatial control over macro-channels and this control leads to increased cell infiltration in vivo. Additionally, due to the versatility of HA scaffolds, we have the potential to control mechanics, degradation, and cell adhesion in this system. In summary, this technology is widely applicable to a range of tissue engineering applications where fibrous systems are desired.

Conclusion

We have developed a process that combines the advantages of electrospinning and photopatterning to obtain scaffolds for tissue engineering applications that exhibit a fibrous structure that mimics the ECM, as well as macro-channels that permit enhanced cellular infiltration and vascularization. This technique overcomes one of the challenges that has plagued the use of fibrous scaffolds, namely the inability of cells to penetrate into the densely packed structures. We showed that the scaffolds maintain their fibrous structure after the photopatterning process and that cellular infiltration is greater when channels are present and the scaffolds are implanted subcutaneously. This technique may find utility for a wide range of tissue engineering applications.

Acknowledgements: The authors would like to acknowledge the experimental assistance of *Derrick Hsu* and *Jamie Ifkovits*. This work was supported by a Fellowship in Science and Engineering from the *David and Lucile Packard Foundation* and a *National Institute of Health* grant R01AR056624.

Received: October 3, 2009; Published online: December 14, 2009; DOI: 10.1002/mabi.200900363

Keywords: biomaterials; electrospinning; hyaluronic acid; photopatterning; photopolymerization

[1] G. M. Whitesides, *Nature* **2006**, *442*, 368.
[2] H. G. Sundararaghavan, G. A. Monteiro, B. L. Firestein, D. I. Shreiber, *Biotechnol. Bioeng.* **2009**, *102*, 632.
[3] M. S. Hahn, L. J. Taite, J. J. Moon, M. C. Rowland, K. A. Ruffino, J. L. West, *Biomaterials* **2006**, *27*, 2519.
[4] S. H. Lee, J. J. Moon, J. L. West, *Biomaterials* **2008**, *29*, 2962.
[5] S. H. Park, T. G. Kim, H. C. Kim, D. Y. Yang, T. G. Park, *Acta Biomater.* **2008**, *4*, 1198.
[6] B. M. Baker, A. O. Gee, R. B. Metter, A. S. Nathan, R. A. Marklein, J. A. Burdick, R. L. Mauck, *Biomaterials* **2008**, *29*, 2348.
[7] A. R. Tan, J. L. Ifkovits, B. M. Baker, D. M. Brey, R. L. Mauck, J. A. Burdick, *J. Biomed. Mater. Res. A* **2008**, *87*, 1034.
[8] G. C. Engelmayr, Jr., M. Cheng, C. J. Bettinger, J. T. Borenstein, R. Langer, L. E. Freed, *Nat. Mater.* **2008**, *7*, 1003.
[9] A. Salerno, M. Oliviero, E. Di Maio, S. Iannace, P. A. Netti, *J. Mater. Sci. Mater. Med.* **2009**, *20*, 2043.
[10] H. Studenovska, M. Slouf, F. Rypacek, *J. Mater. Sci. Mater. Med.* **2008**, *19*, 615.
[11] S. Selvam, W. V. Chang, T. Nakamura, D. M. Samant, P. B. Thomas, M. D. Trousdale, A. K. Mircheff, J. E. Schechter, S. C. Yiu, *Tissue Eng. Part C Methods* **2009**, *15*, 463.
[12] E. S. Place, N. D. Evans, M. M. Stevens, *Nat. Mater.* **2009**, *8*, 457.
[13] B. D. Ratner, S. J. Bryant, *Annu. Rev. Biomed. Eng.* **2004**, *6*, 41.
[14] M. E. Davis, P. C. Hsieh, A. J. Grodzinsky, R. T. Lee, *Circ. Res.* **2005**, *97*, 8.
[15] J. Nam, Y. Huang, S. Agarwal, J. Lannutti, *Tissue Eng.* **2007**, *13*, 2249.
[16] M. F. Leong, M. Z. Rasheed, T. C. Lim, K. S. Chian, *J. Biomed. Mater. Res. A* **2009**, *91*, 231.
[17] Y. Zhang, H. Ouyang, C. T. Lim, S. Ramakrishna, Z. M. Huang, *J. Biomed. Mater. Res. B Appl. Biomater.* **2005**, *72*, 156.
[18] X. Zhu, W. Cui, X. Li, Y. Jin, *Biomacromolecules* **2008**, *9*, 1795.
[19] S. A. Theron, E. Zussman, A. L. Yarin, *Polymer* **2004**, *45*, 2017.
[20] S. Kazemnejad, A. Allameh, M. Soleimani, A. Gharehbaghian, Y. Mohammadi, N. Amirizadeh, M. Jazayery, *J. Gastroenterol. Hepatol.* **2009**, *24*, 278.
[21] R. R. Klossner, H. A. Queen, A. J. Coughlin, W. E. Krause, *Biomacromolecules* **2008**, *9*, 2947.
[22] Y. Ji, K. Ghosh, X. Z. Shu, B. Li, J. C. Sokolov, G. D. Prestwich, R. A. Clark, M. H. Rafailovich, *Biomaterials* **2006**, *27*, 3782.
[23] Q. P. Pham, U. Sharma, A. G. Mikos, *Biomacromolecules* **2006**, *7*, 2796.
[24] J. J. Stankus, J. Guan, K. Fujimoto, W. R. Wagner, *Biomaterials* **2006**, *27*, 735.
[25] J. Shi, L. Wang, Y. Chen, *Langmuir* **2009**, *25*, 6015.
[26] D. Sun, C. Chang, S. Li, L. Lin, *Nano Lett.* **2006**, *6*, 839.
[27] S. J. Bryant, J. L. Cuy, K. D. Hauch, B. D. Ratner, *Biomaterials* **2007**, *28*, 2978.
[28] K. A. Smeds, A. Pfister-Serres, D. Miki, K. Dastgheib, M. Inoue, D. L. Hatchell, M. W. Grinstaff, *J. Biomed. Mater. Res.* **2001**, *54*, 115.
[29] J. B. Leach, K. A. Bivens, C. N. Collins, C. E. Schmidt, *J. Biomed. Mater. Res. A* **2004**, *70*, 74.
[30] J. A. Burdick, C. Chung, X. Jia, M. A. Randolph, R. Langer, *Biomacromolecules* **2005**, *6*, 386.
[31] S. Sahoo, C. Chung, S. Khetan, J. A. Burdick, *Biomacromolecules* **2008**, *9*, 1088.
[32] J. Li, A. He, J. Zheng, C. C. Han, *Biomacromolecules* **2006**, *7*, 2243.
[33] C. Yao, X. Li, T. Song, *J. Biomater. Sci. Polym. Ed.* **2007**, *18*, 731.
[34] S. Khetan, J. S. Katz, J. A. Burdick, *Soft Matter* **2009**, *5*, 1601.
[35] J. L. Ifkovits, J. A. Burdick, *Tissue Eng.* **2007**, *13*, 2369.

DOI: 10.1002/mabi.200900363